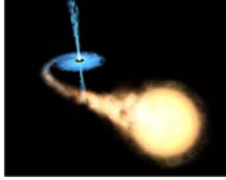

Survey of Micro Quasars

WIKIPEDIA
The Free Encyclopedia

navigation

- Main Page
- Community Portal
- Featured articles
- Current events
- Recent changes
- Random article
- Help
- Contact Wikipedia
- Donations

search

Go Search

Sign in / create account

article discussion edit this page history

Your continued donations keep Wikipedia running!

Microquasar

From Wikipedia, the free encyclopedia

Microquasars are smaller cousins of quasars. They are named after quasars, as they have some common characteristics: strong and variable radio emission often seen as radio jets, and an accretion disk surrounding a black hole. In quasars, the black hole is supermassive (millions of solar masses); in microquasars, the black hole mass is a few solar masses. In microquasars, the accreted mass comes from a normal star and the accretion disk is very luminous in optical regions and X-rays. Microquasars are sometimes called 'radio-jet X-ray binaries' to distinguish them from other X-ray binaries. A part of the radio emission comes from relativistic jets, often showing apparent superluminal motion.

Microquasars are very important for the study of relativistic jets. The jets are formed close to the black hole, and timescales near the black hole are proportional to the mass of the black hole. Therefore, ordinary quasars take centuries to go through variations a microquasar experiences in one day.

See also

[edit]

- SS_433

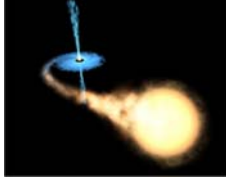

Outline

- Reminder: what is a microquasar?
- Established and Candidate microquasars
- Gamma ray candidates:
  - LSI +615, LS 5039
  - As seen in DC2
- Models for gamma ray spectra

What and Where

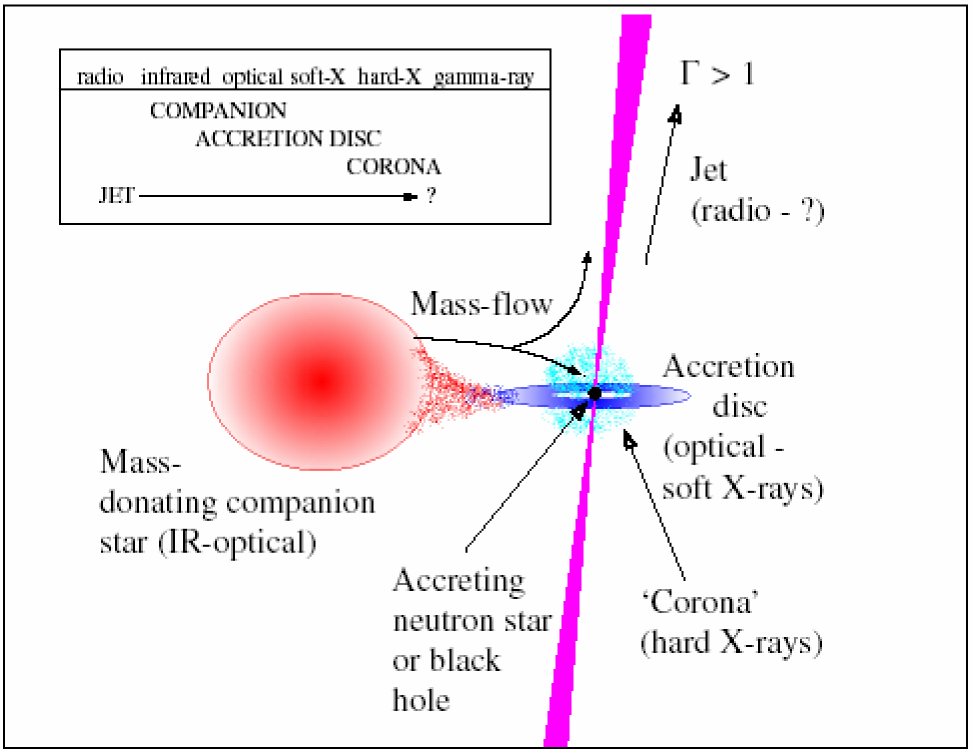

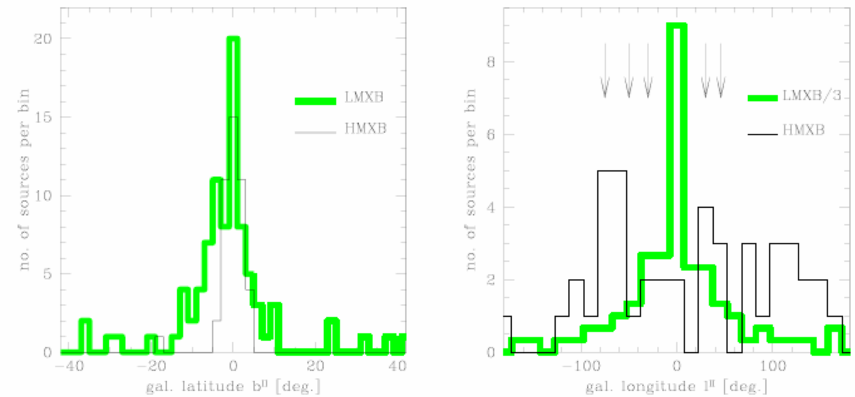

Figure 2.3: *Angular distribution of galactic HMXBs (solid lines) and LMXBs (thick green lines) against the galactic latitude (left panel) and longitude (right panel). These two graphs illustrate the well-known fact that HMXBs are strongly concentrated towards the galactic plane. An important difference in the longitude distributions of HMXBs and LMXBs can be noticed, with the second ones significantly concentrated towards the galactic center/bulge and the former distributed in clumps approximately coinciding with the location of tangential points of the spiral arms (whose position is marked by arrows in the right panel). The LMXBs number is divided by 3 on the right panel (from Grimm et al. 2002).*

High Mass XRB live near galactic plane
Low Mass XRB live in the bulge

microQuasar ≡ X-ray binary with jets

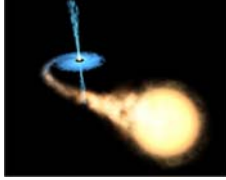

Candidate Microquasars

Table 2.1: Microquasars in our Galaxy

Name	Position (J2000.0)	System type[a]	D (kpc)	P_{orb} (d)	$M_{compact}$ ($M_\odot$)	Activity radio[b]	β_{app}	θ[c]	Jet size (AU)	Remarks[d]
High Mass X-ray Binaries										
* LS I +61 303	$02^h40^m31^s.66$ $+61°13'45''.6$	B0V +NS?	2.0	26.5	–	p	$\geq$0.4	–	10–700	Prec?
V4641 Sgr	$18^h19^m21^s.48$ $-25°25'36''.0$	B9III +BH	$\sim$ 10	2.8	9.6	t	$\geq$ 9.5	–	–	
* LS 5039	$18^h26^m15^s.05$ $-14°50'54''.24$	O6.5V((f)) +NS?	2.9	4.1	1–3	p	$\geq$ 0.15	$<81°$	$10–10^3$	Prec?
SS 433	$19^h11^m49^s.6$ $+04°58'58''$	evolved A? +BH?	4.8	13.1	11±5?	p	0.26	79°	$\sim 10^4–10^6$	Prec XRJ
Cygnus X-1	$19^h58^m21^s.68$ $+35°12'05''.8$	O9.7Iab +BH	2.5	5.6	10.1	p	–	40°	$\sim$ 40	Prec?
* Cygnus X-3	$20^h32^m25^s.78$ $+40°57'28''.0$	WNe +BH?	9	0.2	–	p	0.69	73°	$\sim 10^4$	
Low Mass X-ray Binaries										
XTE J1118+480	$11^h18^m10^s.85$ $+48°02'12''.9$	K7V–M0V +BH	1.9	0.17	6.9±0.9	t	–	–	$\leq$ 0.03	
Circinus X-1	$15^h20^m40^s.9$ $-57°10'01''$	Subgiant +NS	5.5	16.6	–	t	>15	$<6°$	$>10^4$	
XTE J1550−564	$15^h50^m58^s.70$ $-56°28'35''.2$	G8–K5V +BH	5.3	1.5	9.4	t	>2	–	$\sim 10^{3*}$	XRJ
Scorpius X-1	$16^h19^m55^s.1$ $-15°38'25''$	Subgiant +NS	2.8	0.8	1.4	p	0.68	44°	$\sim$ 40	
* GRO J1655−40	$16^h54^m00^s.25$ $-39°50'45''.0$	F5IV +BH	3.2	2.6	7.02	t	1.1	72°–85°	$8\ 10^3$	Prec?
GX 339−4	$17^h02^m49^s.5$ $-48°47'23''$	– +BH	>6	1.76	5.8±0.5	t	–	–	$\sim 4.6\ 10^{4\dagger}$	
1E 1740.7−2942	$17^h43^m54^s.83$ $-29°44'42''.60$	– +BH ?	8.5?	12.5?	–	p	–	–	$\sim 10^6$	
XTE J1748−288	$17^h48^m05^s.06$ $-28°28'25''.8$	– +BH?	$\geq$ 8	?	>4.5?	t	1.3	–	$>10^4$	
GRS 1758−258	$18^h01^m12^s.40$ $-25°44'36''.1$	– +BH ?	8.5?	18.5?	–	p	–	–	$\sim 10^6$	
GRS 1915+105	$19^h15^m11^s.55$ $+10°56'44''.7$	K–M III +BH	12.5	33.5	14±4	t	1.2-1.7	66°-70°	$\sim 10–10^4$	Prec?

Notes: [a] NS: neutron star; BH: black hole. [b] p: persistent; t: transient. [c] jet inclination. [d] Prec: precession; XRJ: X-ray jet. *Reported by Corbel et al. 2002. †Recently reported by Gallo et al. 2004.

* - γ-ray candidates

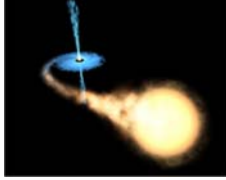

LS 5039 & LS I +613

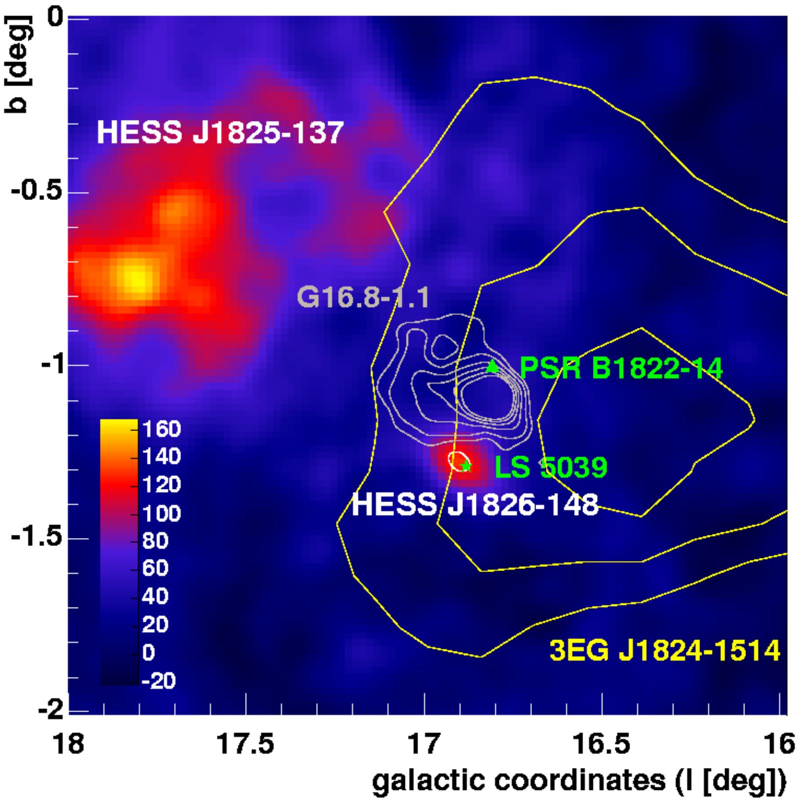

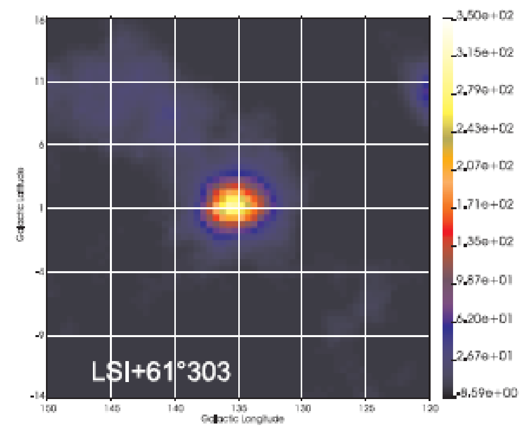

Φ = 35.2 x 10^{-8} $cm^{-2}s^{-1}$ E>100 MeV
Γ= 2.2

HESS: Γ=2.12

2EG J0431+6119 (aka 3EG J0435+6137)

Φ = 9.2±0.6 x 10^{-7} $cm^{-2}s^{-1}$ E>100 MeV
Γ= 2.46

Not visible by HESS

HESS: Detected again this year

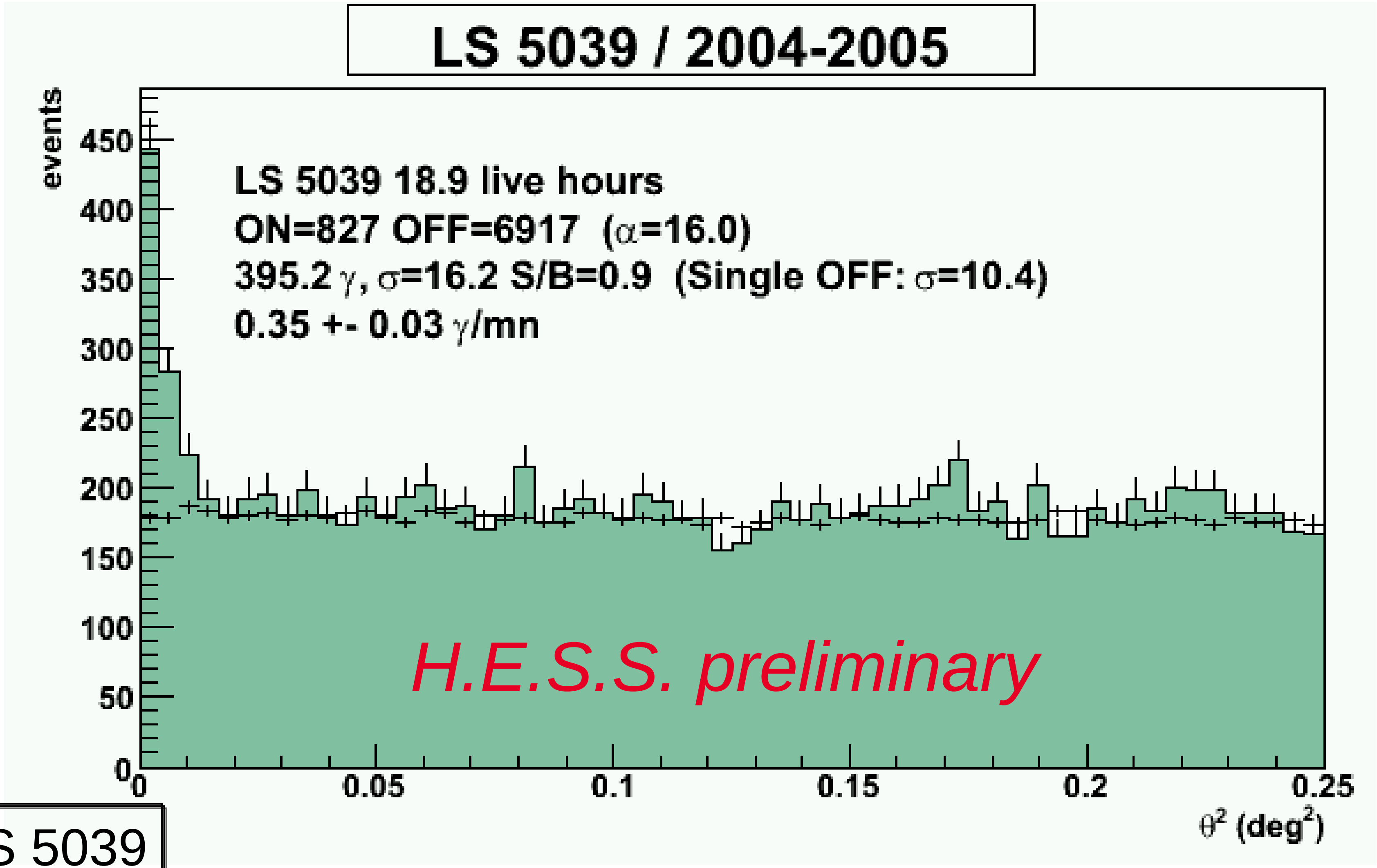

LS 5039

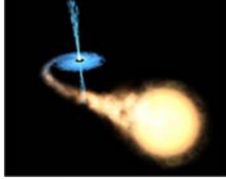

H.E.S.S. lightcurve (2004)

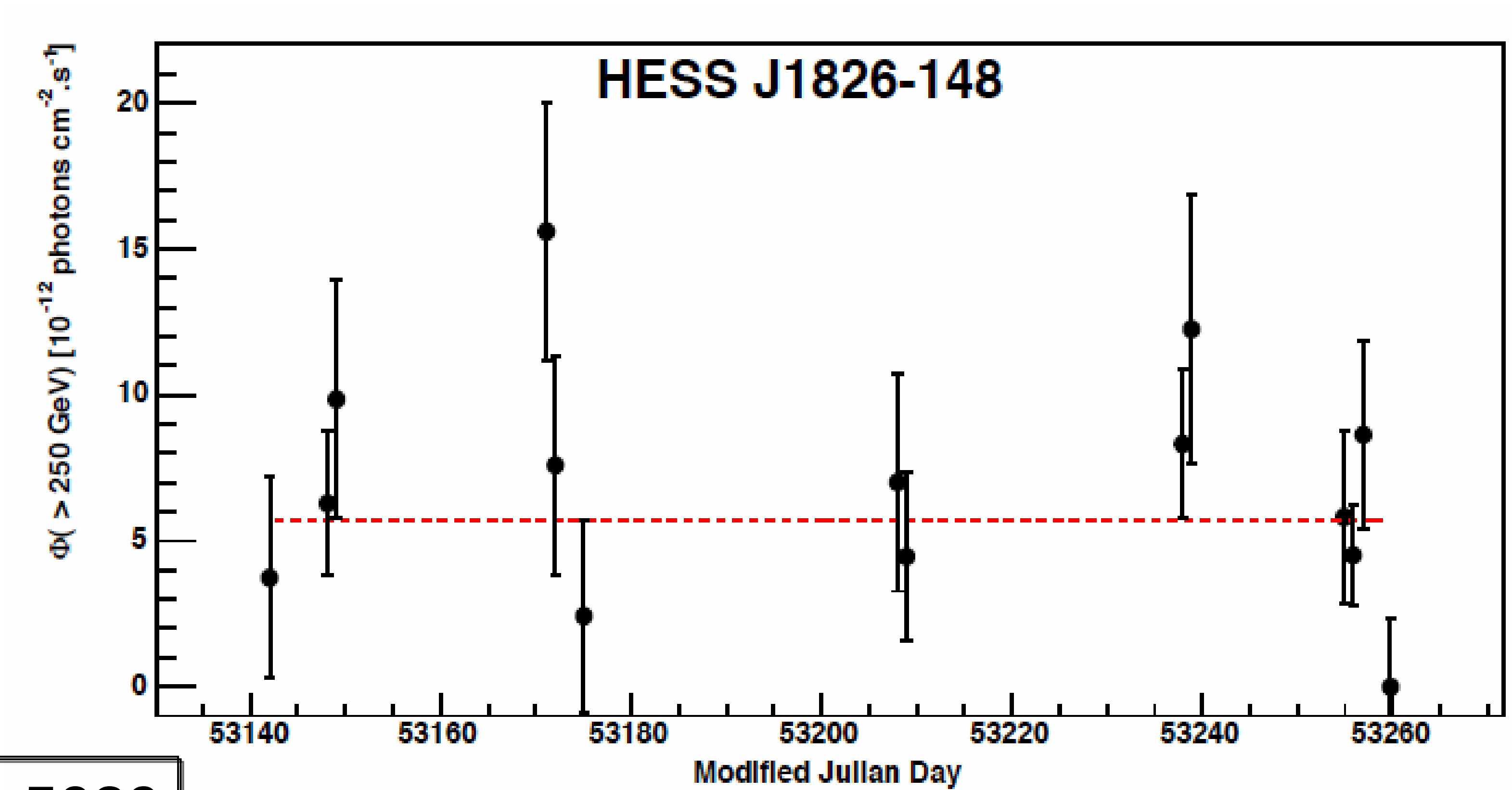

LS 5039

No significant variations

Aharonian et al., Science 309(746), 2005

H.E.S.S. spectrum: hard

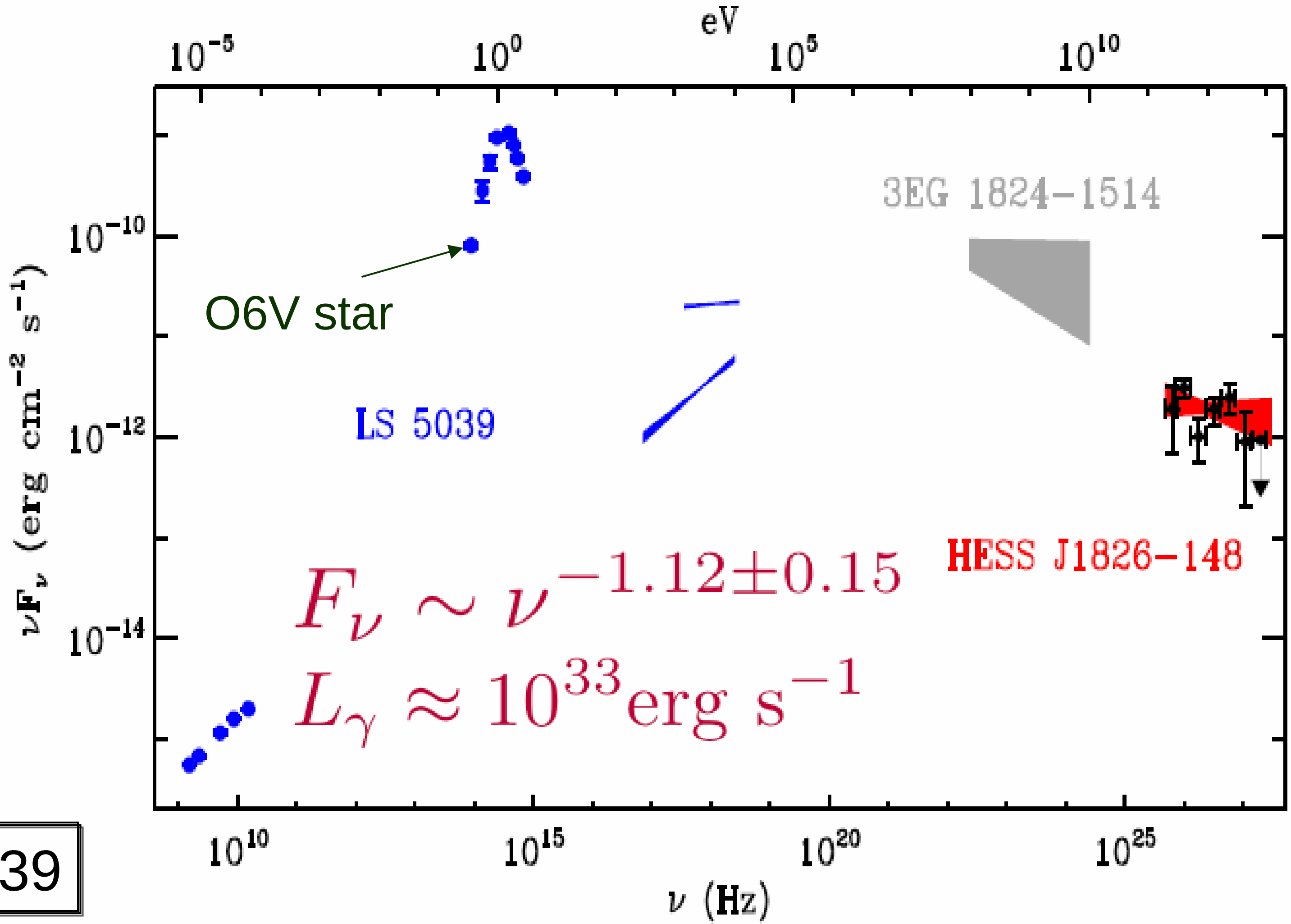

LS 5039

Aharonian et al., Science 309(746), 2005

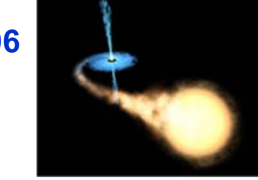

LS 5039, LS I +615 & Friends Candidates in DC2

Toby’s HEALPIX map + Saclay sources

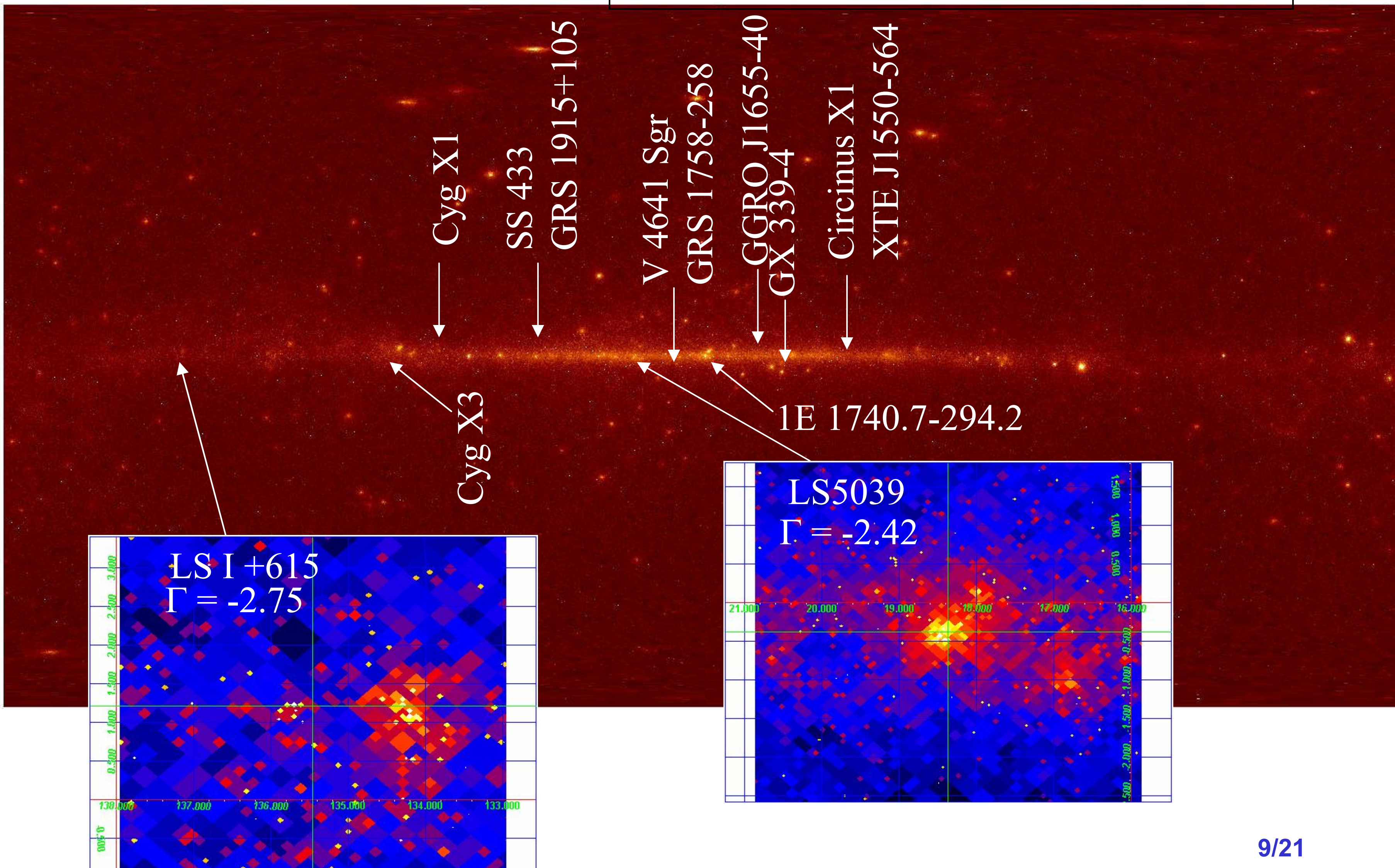

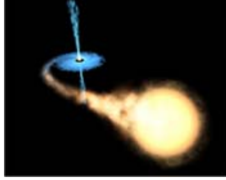

Models for γ-ray Emission

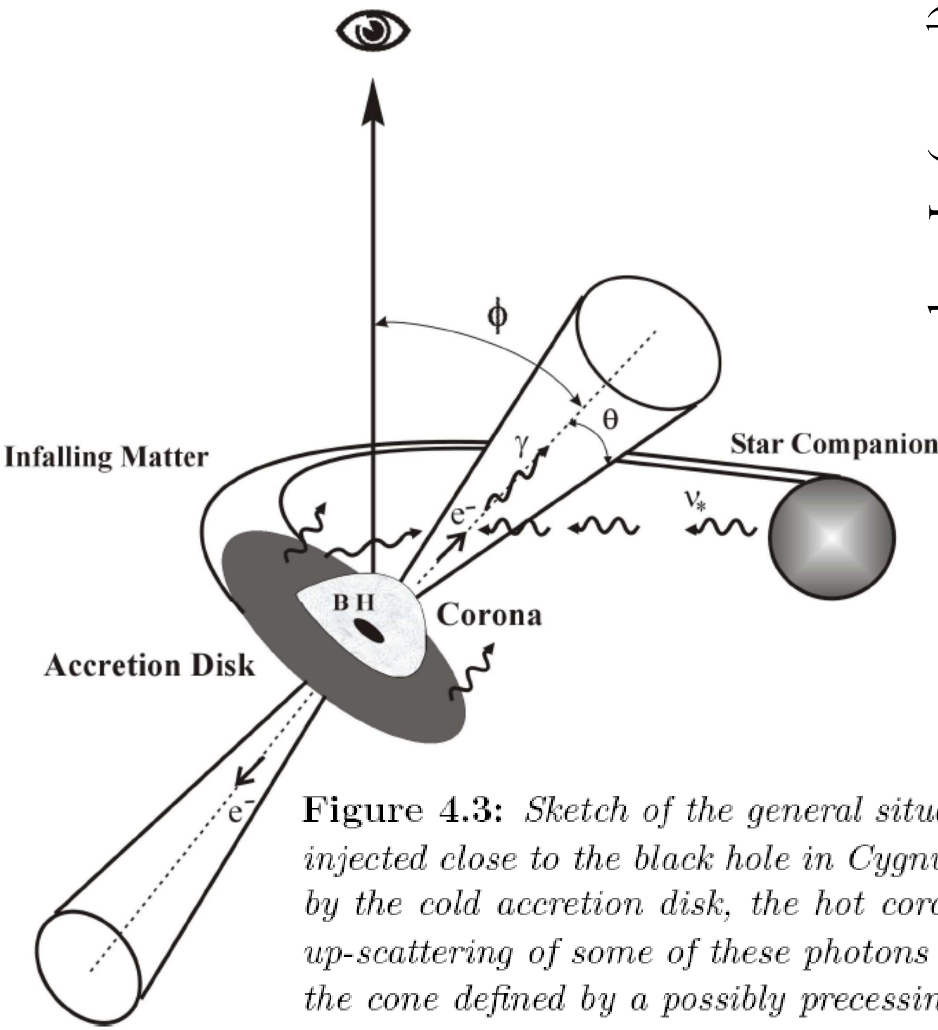

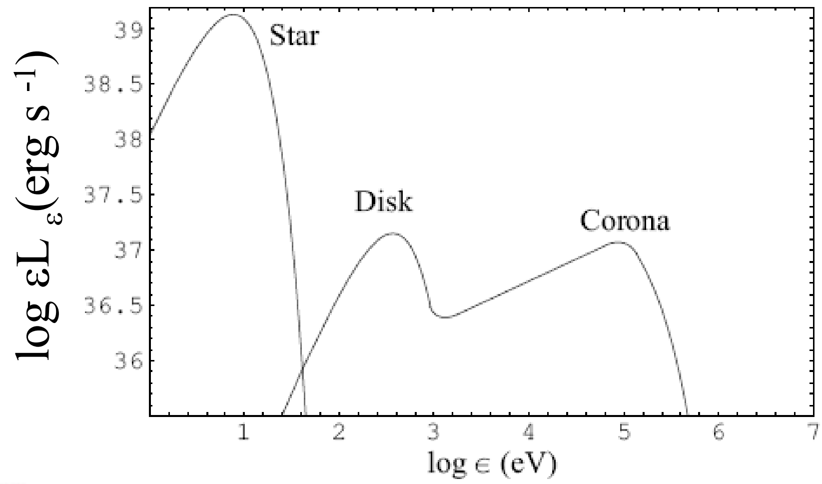

Figure 4.1: *External photon fields to which the jet is exposed.*

Figure 4.3: *Sketch of the general situation discussed in this chapter. A relativistic jet is injected close to the black hole in Cygnus X-1. This jet must traverse photon fields created by the cold accretion disk, the hot corona, and the stellar companion. Inverse Compton up-scattering of some of these photons is unavoidable. Here θ is the half-opening angle of the cone defined by a possibly precessing jet.*

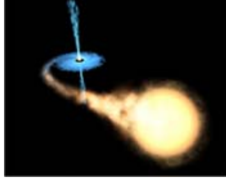

Standard Disk Model: Star, Disk, Corona

- Star
  - blackbody – T ~ 10^4K – peak @ kT – E ~ 10 eV

- Accretion Disk
  - Energy emission due to angular momentum transport
  - Inner radius ~$3r_s \approx 9\ M_x$ km (eg 18 km for 2 solar masses)
    - T_{in} ~ 2 $10^7\ M_x^{-1/4}$ K
    - 1 solar mass → 10M K → ~ 1 keV
    - Integrate radial temp spectrum

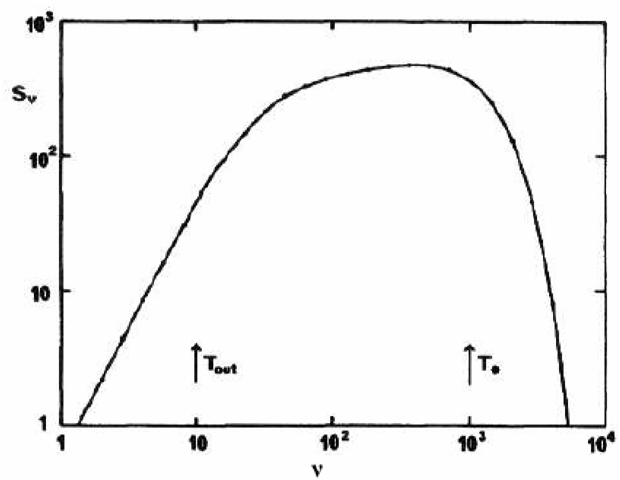

Figure 2.5: *The integrated spectrum of a steady accretion disk that radiates a local black-body spectrum at each point. The units are arbitrary, but the frequencies corresponding to* $T_{out} = T(R_{out})$ *and* T_* *are marked (from Pringle 1981).*

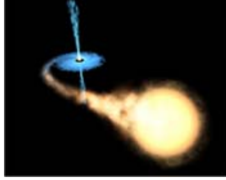

Standard Disk Model: Hard X-rays

- Observations show hard x-ray spectra
  - Requires 10^9 K
  - Hence postulate corona

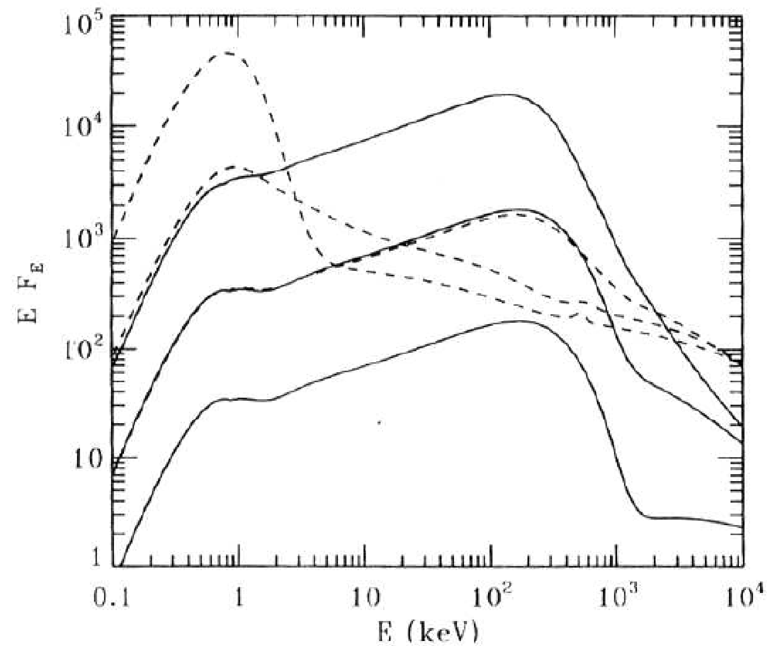

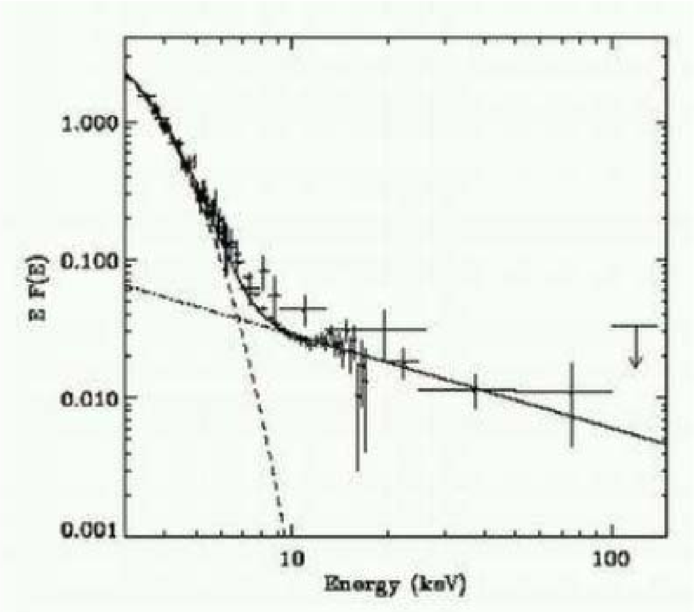

Figure 12: **Spectrum of XTE J1720-318 in a Soft state.** Cadolle Bel et al. 2004. Dashed: Multicolor Disk with R_{in}=84 km. Dotted dashed: Power law photon index 2.6 Thick: Total model.

Figure 2.7: *Spectra from the hybrid pair plasmas. Solid curves show dependence on hard compactness* l_h. *Other parameters:* $l_h/l_s = 10$, $l_{nth}/l_h = 0.1$, $\tau_p = 1$, $\Gamma_{inj} = 2.5$, $T_{bb} = 0.2$ *keV. The resulting electron temperature and optical depth are* (kT_e, τ_T)*=(126 keV, 1.0002), (123 keV, 1.02), and (82 keV, 1.47) for* l_h *= 1, 10, 100, respectively (*l_h *increases from the bottom to the top of the figure). For a higher compactness, the spectrum has a sharper cut-off at energies above 1 MeV due to larger optical depth for photon-photon pair production. These spectra are similar to the spectra of Galactic BHs in their hard state. Dashed curves show dependence on* l_h/l_s. *Here we fixed* $l_h = 10$, $l_{nth}/l_h = 0.5$. *The resulting electron temperature and optical depth* (kT_e, τ_T) *are (104 keV, 1.07), (34 keV, 1.02), and (5 keV, 1.01) for* $l_h/l_s = 10, 1, 0.1$, *respectively. Increase in* l_h *results in a more pronounced blackbody part of the emerging spectrum. The blackbody is modified by Comptonization on thermal electrons (from Poutanen 1998).*

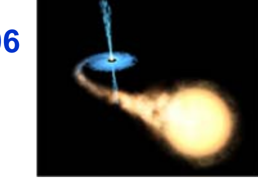

Dynamics in Disk-Jet System

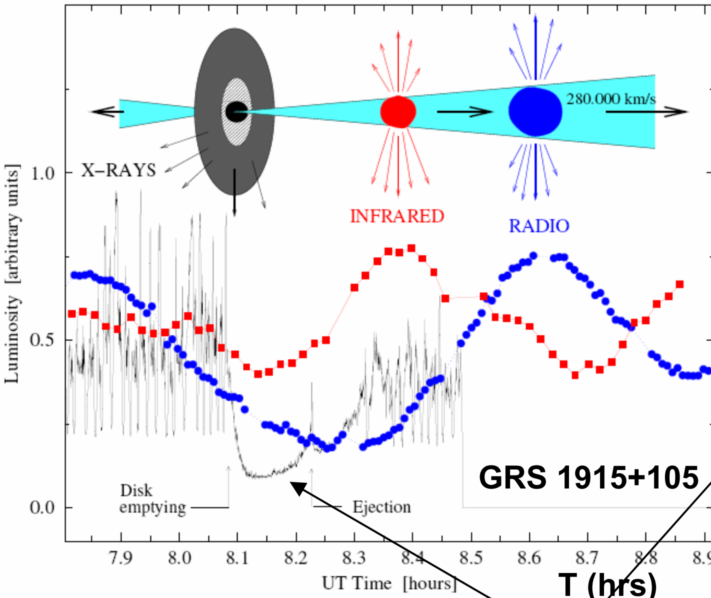

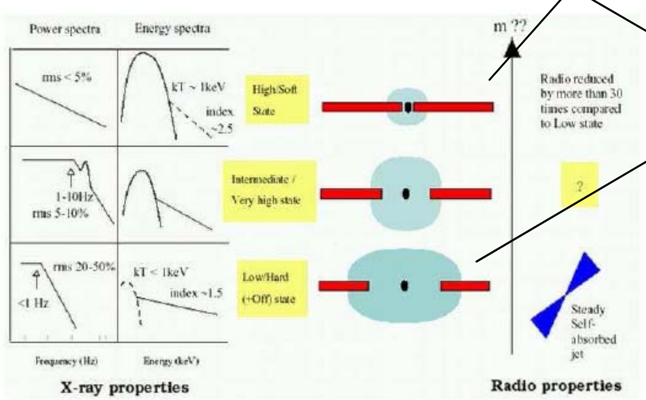

Figure 10: **The X-ray states of a black hole .** Left: The states are defined by the spectral and timing properties. Right: Morphology of the accretion disk/Corona and radio properties during the X-ray states (Fender 2002).

High luminosity from inner disk;
Soft x-rays

Low luminosity from corona;
Hard x-rays

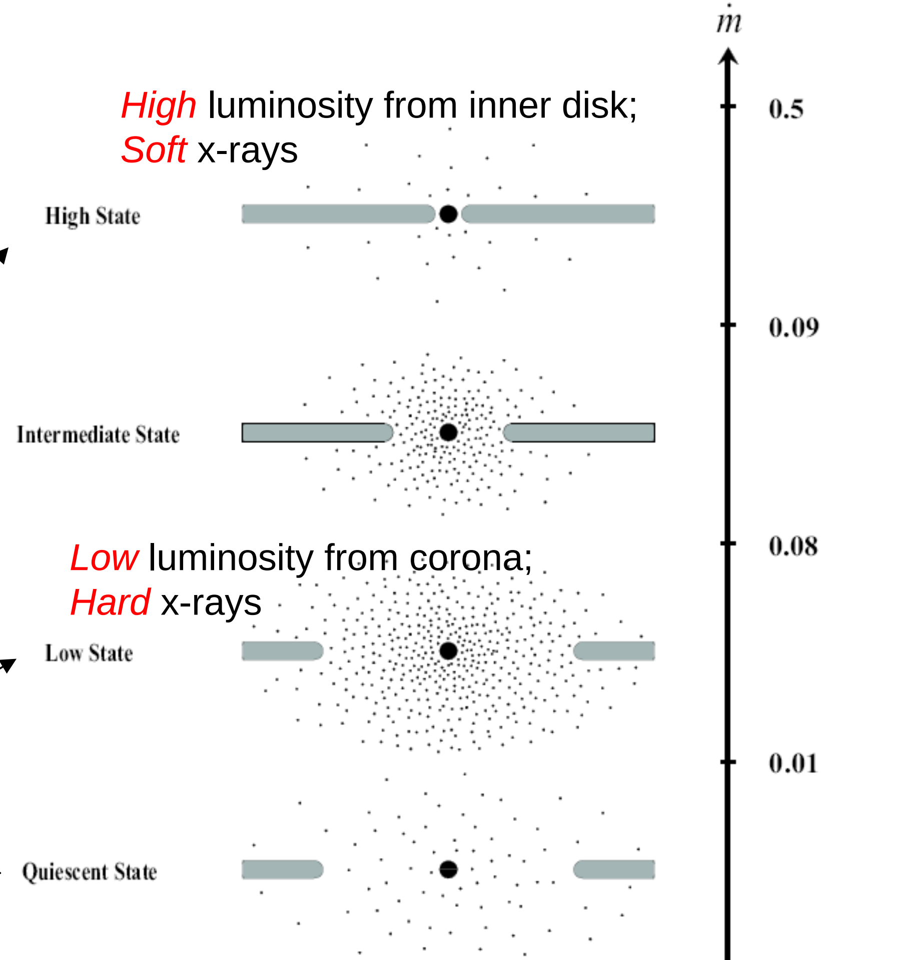

Figure 2.10: *The configuration of the accretion flow in different spectral states shown schematically as a function of the total mass accretion rate $\dot{m}$. The coronal region is indicated by dots and the thin disk by horizontal bars. (Adapted from Esin et al. 1997)*

Jet Observations

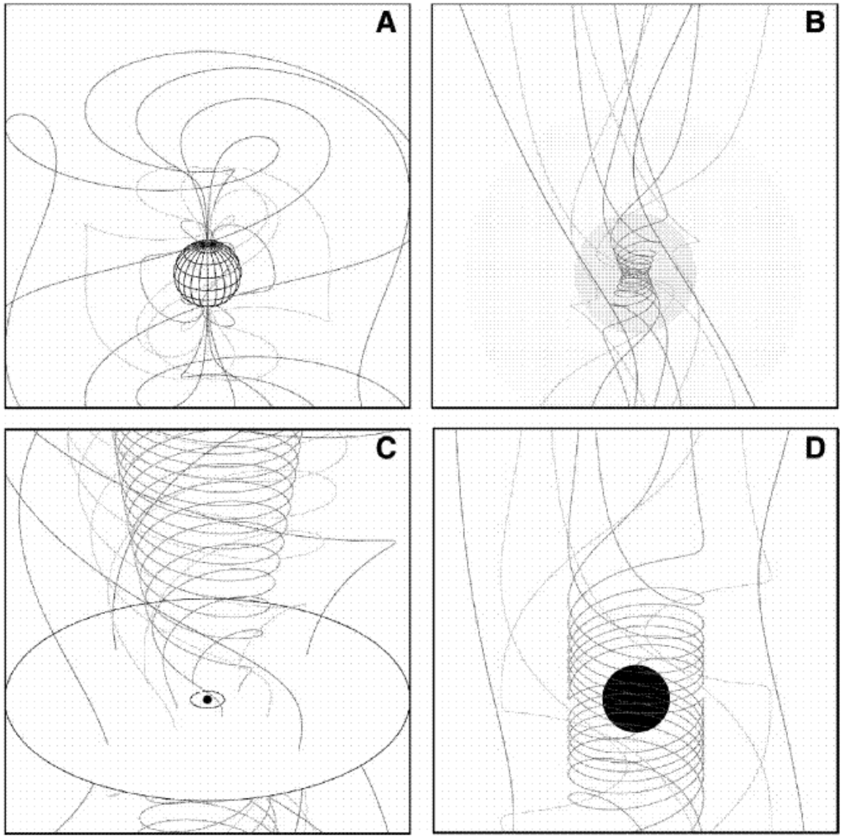

Figure 2.9: *Four ways to make jets with magnetic fields. A: dipole field of a rotating neutron star. B: A collapsing object drawing and winding up an initially uniform field. C: Poloidal magnetic field from a magnetized accretion disk. D: Frame-dragging near a rotating black hole resulting in strong coiling of the magnetic field lines. Types C and D (possibly also A) may be relevant for X-ray binaries; type A for isolated pulsars; types C and D for AGN (from Meier et al. 2001).*

- μQ jets too small to image anytime soon
- complicated MHD calculations!

- practical models of jets used in calcs:
    - inject blobs of plasma at some height above the disk, bulk Lorentz Γ (eg 5)
    - isotropic lepton spectrum in blob, power law (-2) with min, max γ corresponding to inferred max E in TeV range

Jet Interactions with Stellar Photon Field

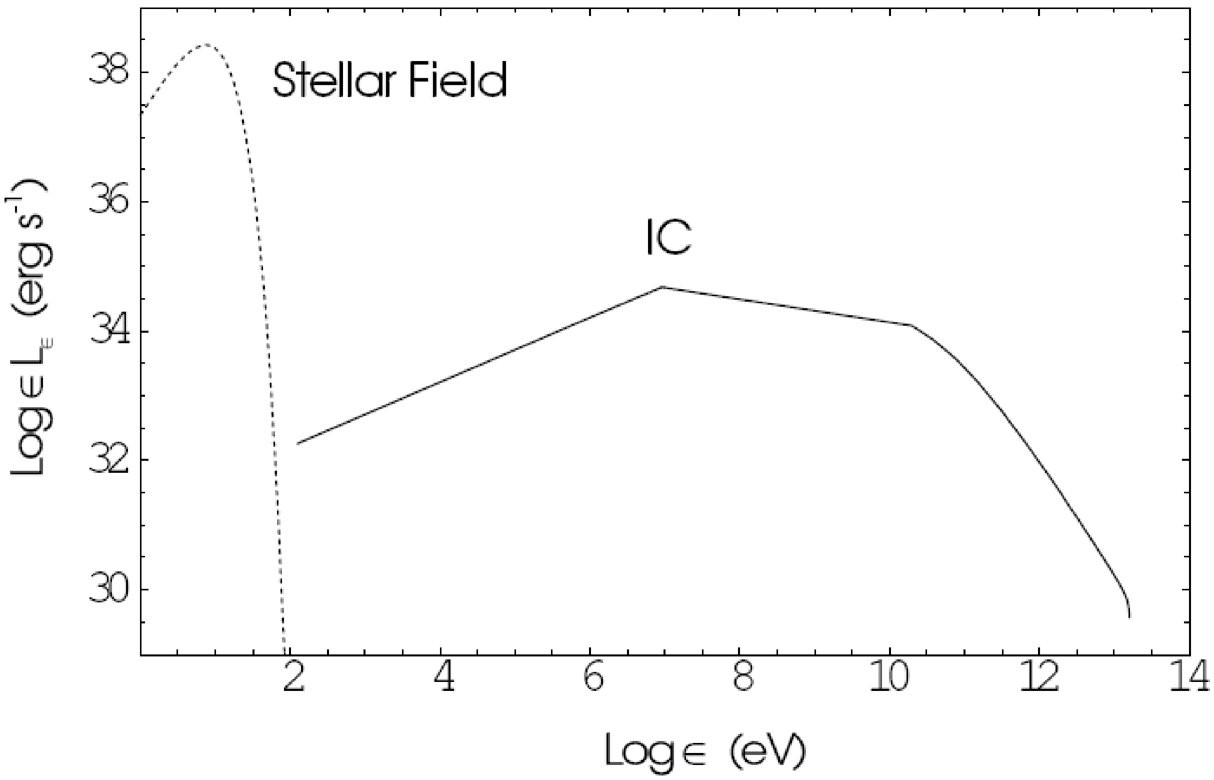

Figure 3.2: *Inverse-Compton spectral energy distribution for a microquasar with a massive stellar companion. Leptons in the jet are assumed to have a power-law energy distribution with an index $p = 2$ and a high-energy cut-off at multi-TeV energies. Notice the softening of the spectrum at high-energies due to the Klein-Nishina effect.*

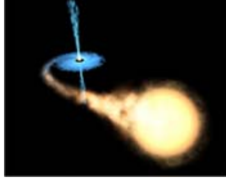

Jet Interactions with Disk, Corona

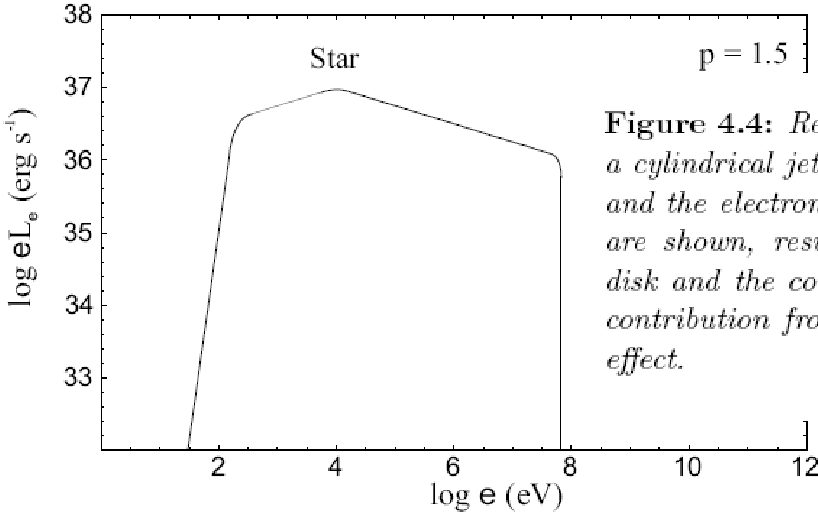

Figure 4.4: *Results of the model for an injection electron spectrum with index $p = 1.5$ in a cylindrical jet forming a viewing angle of 30 degrees. The bulk Lorentz factor is $\Gamma = 5$ and the electron power law extends from $\gamma_1 = 2$ to $\gamma_2 = 10^3$. Three different components are shown, resulting from the up-scattering of photons from the star (top panel), the disk and the corona (bottom panel, solid and dashed lines respectively). Notice that the contribution from the coronal photons is not a power law because of the Klein-Nishina effect.*

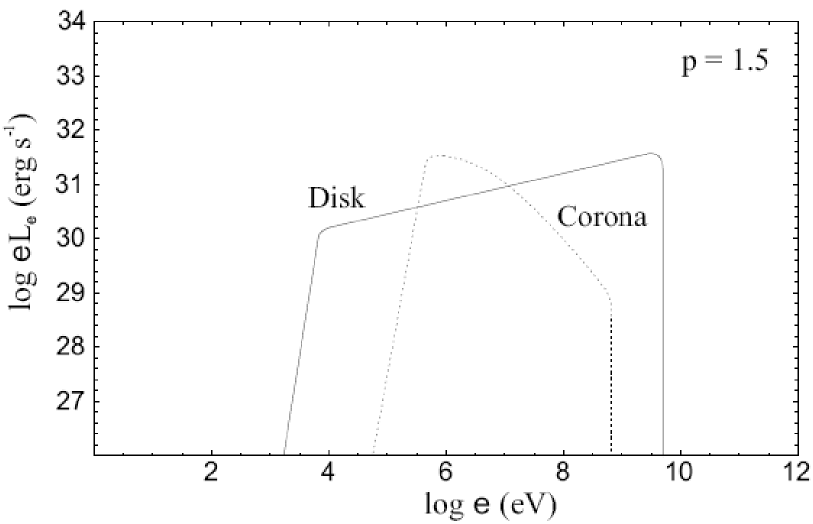

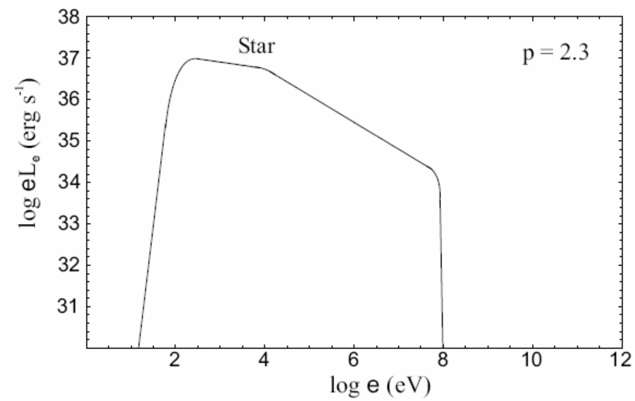

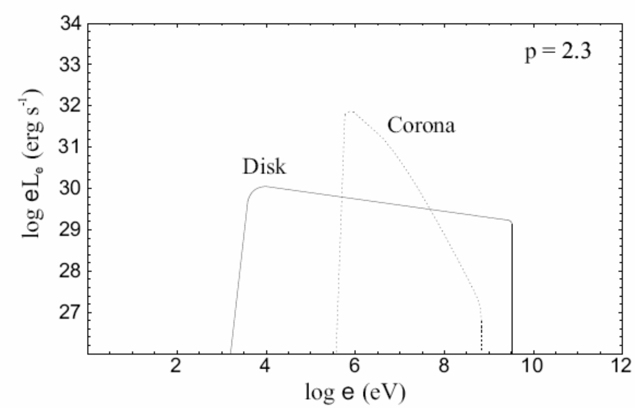

R.Dubois

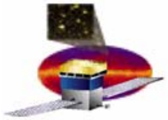

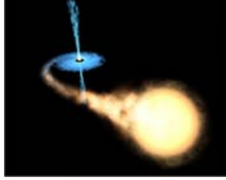

Leptonic Jet Models

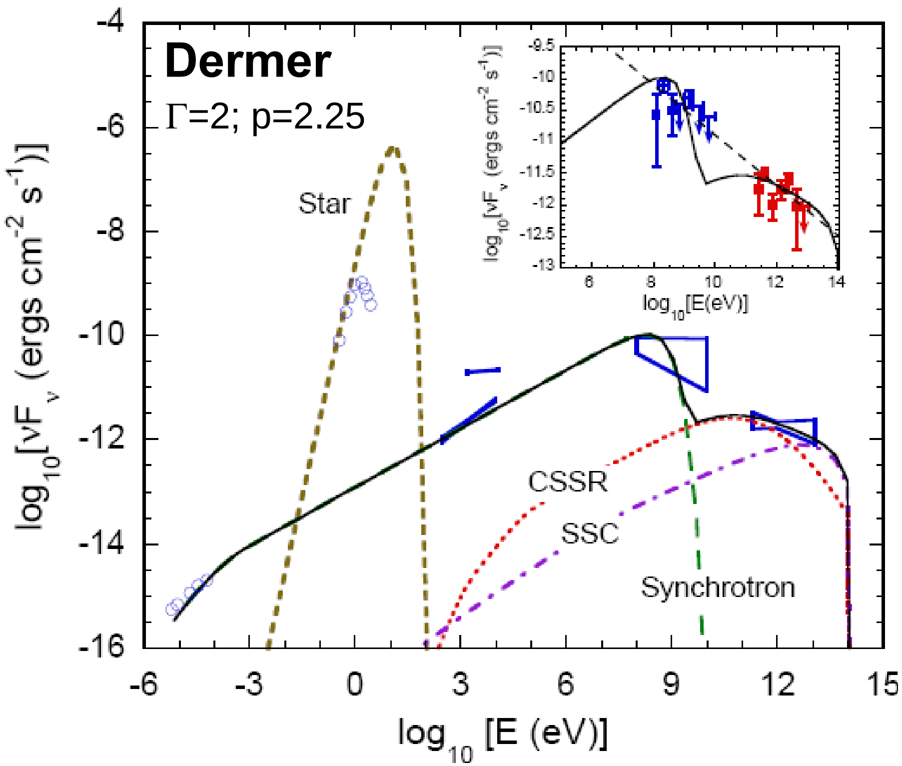

• Inverse compton from star dominates at high energy

• ignores variability and non-contemporaneous measurements

R.Dubois

Includes $\gamma\gamma$ annihilation with stellar field

6 Paredes, Bosch-Ramon & Romero: Broad-band emission from LS 5039

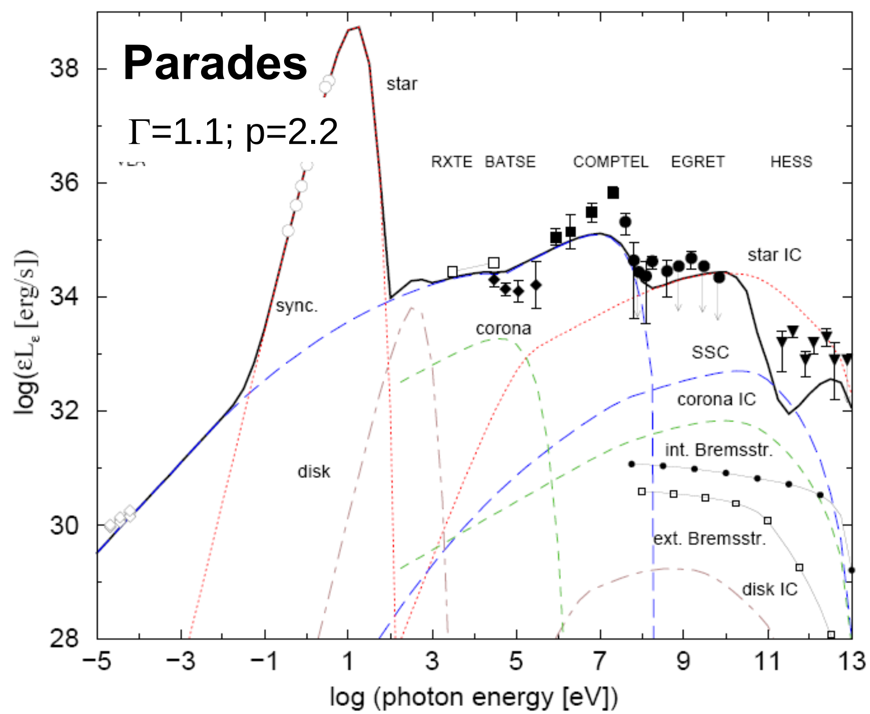

Fig. 3. Comparison of the spectral energy distribution of LS 5039 computed from the present model, at the periastron passage and using the parameters of Table 1, with the observed data. We show the different components of the emission as well as the sum of all of the them, which is attenuated due to $\gamma\gamma$ absorption (solid line). The points observed are from Martí et al. (1998) (VLA, diamond), Clark et al. (2001) and Drilling (1991) (optical, circle, corrected of absorption), Bosch-Ramon et al. (2005a) (RXTE, square), Harmon et al. (2004) (BATSE, diamond filled), Collmar et al. (2003) (COMPTEL, square filled), Hartman et al. (1999) (EGRET, circle filled) and Aharonian et al. (2005a) (HESS, triangle down filled). The arrows in the EGRET and HESS data represent upper limits (3σ).

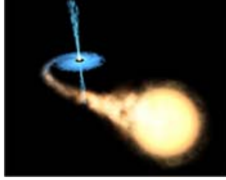

Recall from μQ II: LS 5039 Spectral fit assuming it is a pulsar

G.Dubus

Pulsar wind parameters:
10^{36} erg/s, $\gamma_w=10^6$ and $\sigma=0.001$

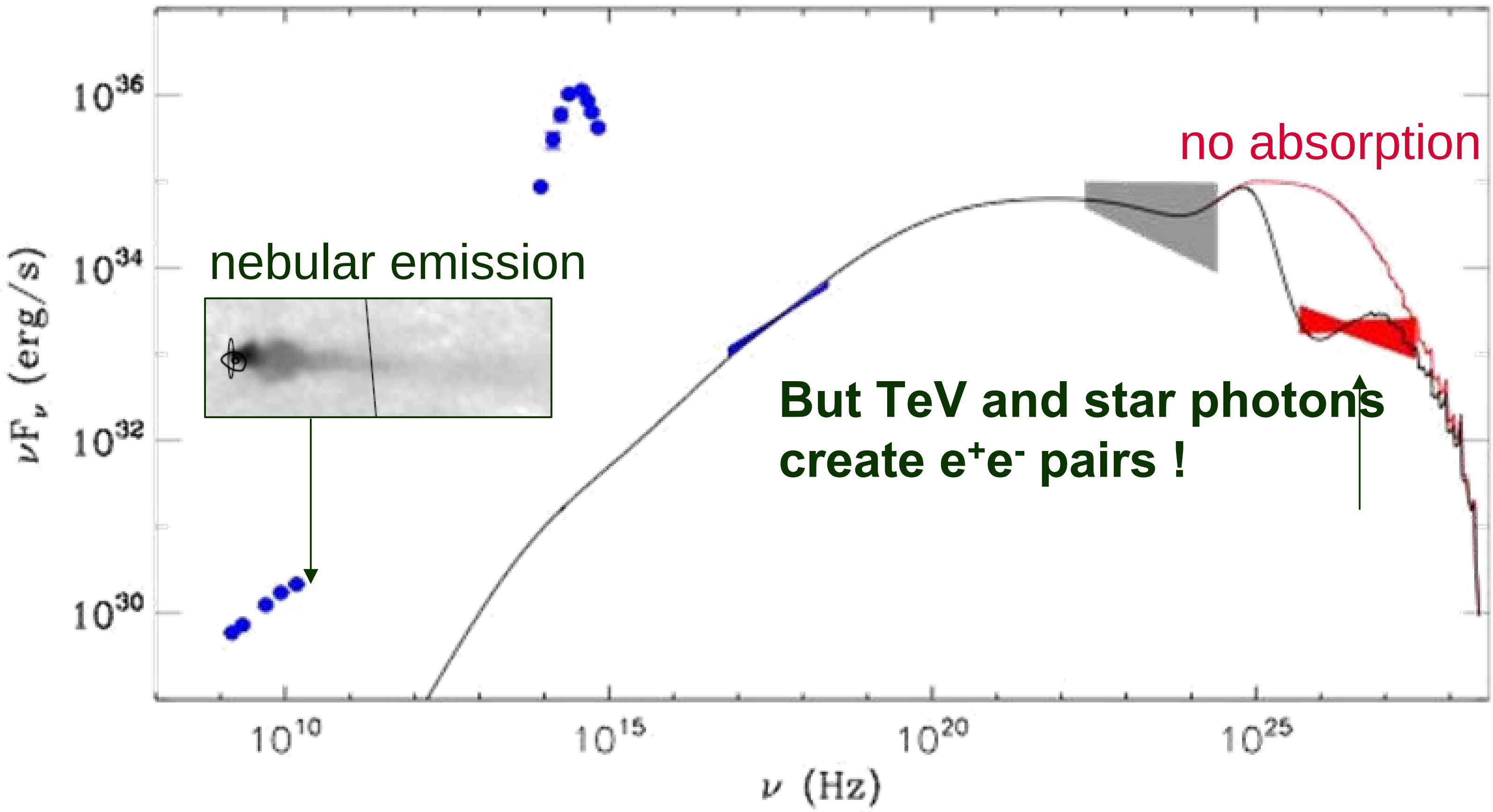

Additional Variability

- Two potential sources:
  - Precession of jet by drag of star gravity on disk
  - Assumed to transmit to jet

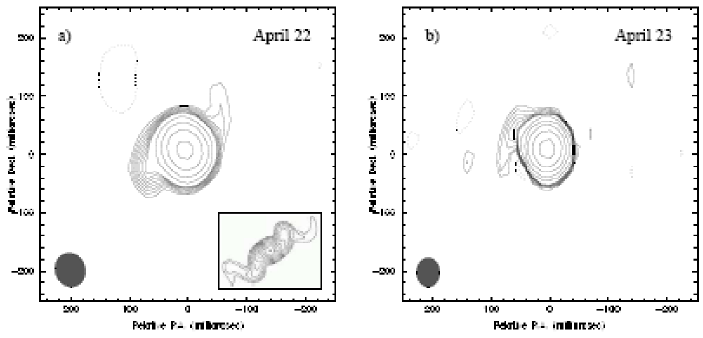

Figure 35: : The precessing jet of LS I +61°303 . Massi et al 2004. a) MERLIN

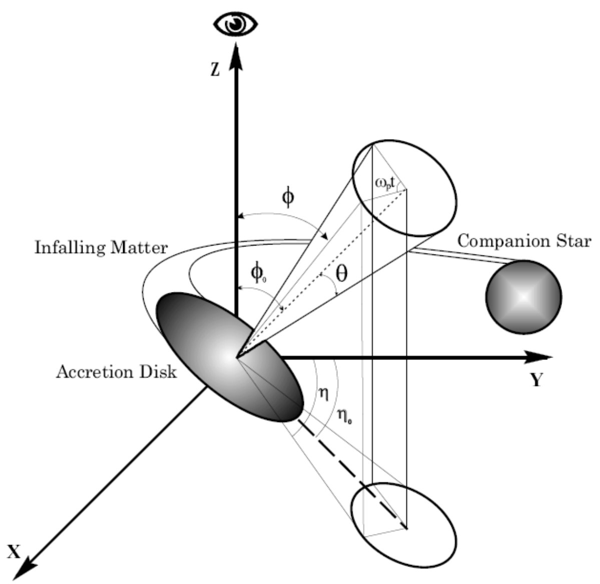

Figure 3.3: *Precessing jet model.*

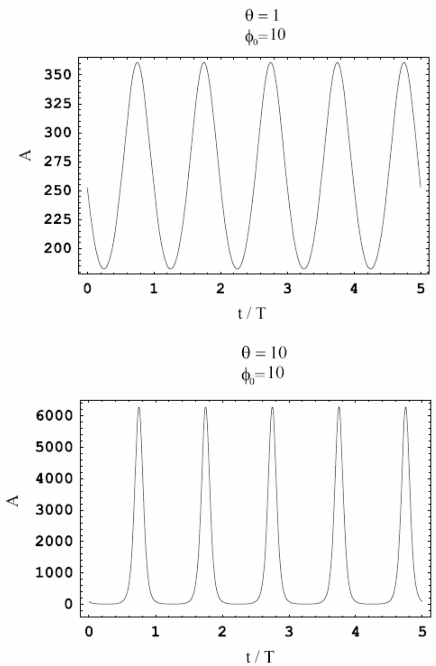

For "LS5039"; $\theta \sim 10^0 \rightarrow$ T~ 100 days

Huge variation depending on angle of jet to disk

GRO J1655-40, V 4641 Sgr show significant misalignments

SS 433 shows 162 day period

Figure 3.4: *Variation of the amplification factor for continuous jet emission as a function of time in the precessing microblazar model (for two different opening angles). Time units are normalized to the precessing period.*

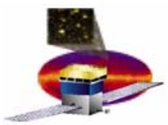

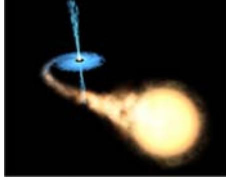

Variability 2

– **Orbital effects on accretion ("two-peak" accretion model) and extinction of γ's by stellar field**

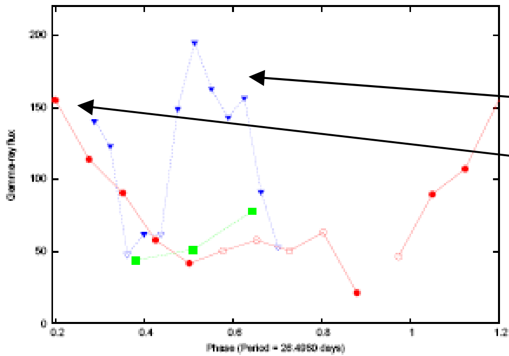

Lower density wind
Lower compact obj speed

High density wind
High compact speed

Figure 31: : **EGRET data vs. orbital Phase** Massi et al 2004b (see text).

Colours represent 3 epochs

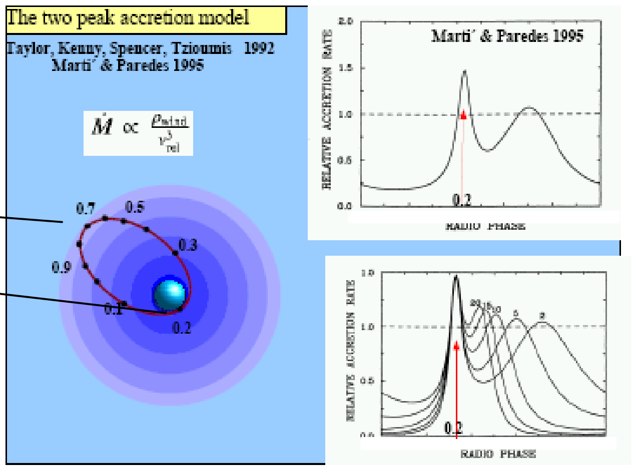

Figure 26: : **The accretion model for an eccentric orbit.** Martí & Paredes 1995. Top: Accretion rate versus stellar wind. The vertical axis is in units of the Eddington accretion limit, whose limit is indicated by the dashed line. Bottom: Accretion rate for different velocities of the stellar wind. The values are in km s^{-1}. Note how the second super-critical event shifts gradually towards earlier orbital phases for high values of the wind velocity.

From μQ II: Extinction at high E due to γγ interactions vs orbital phase

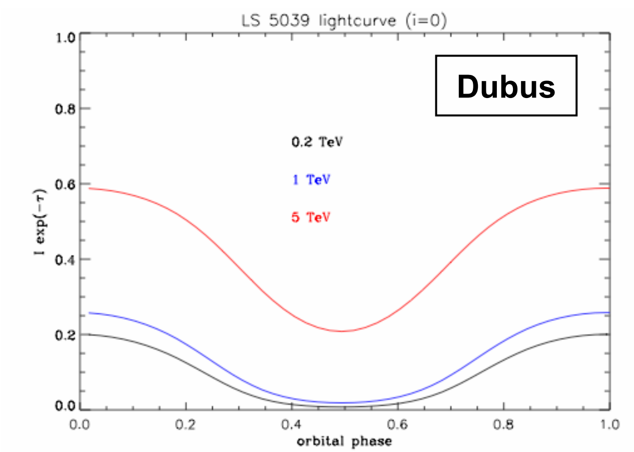

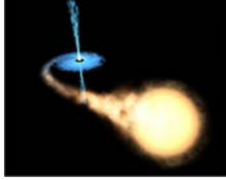

What will GLAST Contribute?

- There is only statistics of TWO for observations in GLAST energy range (LS 5039, LS I +613)
  - And LS 5039 might not even be a microquasar!
- Need more candidates
  - Survey mode should allow us to examine known candidates
  - Hopefully ACTs will see more (eg LS I +613 from some northern telescope?) before we go up
    - Definitive IDs from precise positions, variability
- Keep an eye out for variability
  - MW observations with x-ray, radio
  - Correlate gamma ray variability with disk-jet variations?
  - Untangle precession, orbital effects
  - Hopefully more understanding of disk-jet variations by then